Letter

Non-Hermitian skin effect induced by Rashba-Dresselhaus spin-orbit coupling

Pavel Kokhanchik [ORCID],[1,*] Dmitry Solnyshkov [ORCID],[1,2] and Guillaume Malpuech[1]

[1]*Institut Pascal, Université Clermont Auvergne, CNRS, Clermont INP, F-63000 Clermont–Ferrand, France*
[2]*Institut Universitaire de France (IUF), F-75231 Paris, France*

One-dimensional (1D) chains with nonreciprocal tunneling realizing the non-Hermitian skin effect (NHSE) have attracted considerable interest in the last years, whereas their experimental realization in real space remains limited to a few examples. In this Letter, we propose a generic way of implementing nonreciprocity based on a combination of Rashba-Dresselhauss spin-orbit coupling, existing for electrons, cold atoms, and photons, and a lifetime imbalance between two spin components. We show that one can realize the Hatano-Nelson model, the non-Hermitian Su-Schrieffer-Heeger model, and even observe the NHSE in a 1D potential well without the need for a lattice. We further demonstrate the practical feasibility of this proposal by considering the specific example of a photonic liquid-crystal microcavity. This platform allows one to switch on and off the NHSE by applying an external voltage to the microcavity.

Introduction. The last decades have been marked by a growing interest in non-Hermitian physics [1], which appears reasonable due to the ubiquitous nonequilibrium nature of physical systems. Many phenomena without Hermitian analogs have been found. From a mathematical perspective, these are exceptional points and their nodal phases, non-Hermitian symmetry operators and classes [2], anomalous bulk-boundary correspondence [3] (BBC), and related non-Hermitian skin effect [4] (NHSE). From the physical point of view, these mathematical concepts became a foundation for unidirectional invisibility [5], enhanced sensitivity [6–8], high-performance lasing [9], etc.

The BBC [10–12] relates the topologically nontrivial structure of bulk states with the presence of topologically protected edge states. It relies on the assumption that the introduction of the boundary does not induce any effects on the bulk. While the BBC is valid in Hermitian systems, it was found to be broken in many classes of non-Hermitian systems [3,13–15]. The BBC breakdown is always accompanied by the piling up of the bulk states of the system at the boundary (skin modes), the effect which was dubbed NHSE in analogy with the skin effect in electromagnetism [4,16–18]. The simplest model demonstrating NHSE is the Hatano-Nelson (HN) model [16], a one-dimensional (1D) chain with nonreciprocal couplings. However, the breakdown of BBC cannot be observed in the HN chain since its Hermitian analog, a monomer chain, does not possess edge states. Thus the simplest model where the BBC breakdown was first investigated is the non-Hermitian Su-Schrieffer-Heeger (SSH) model [Fig. 1(d)] [4,18–20], a non-Hermitian extension of a 1D SSH dimer chain possessing topologically protected edge states [21,22]. The two main and complementary ways to restore the BBC were suggested: using special topological invariants for non-Bloch Hamiltonians

of infinite systems [4,23] or calculating the biorthogonal polarization for finite systems with an open boundary condition (OBC) Hamiltonian [18,24,25].

The two frameworks exist as well to describe the NHSE: The first is based on the non-Hermitian winding number calculated for a Bloch Hamiltonian with a periodic boundary condition (PBC) [see Eq. (5)] [26,27]. The other utilizes the concept of the generalized Brillouin zone (GBZ) [23,28]. Even though the two approaches are equivalent [29], combining both is helpful to visualize the complementary information about the system eigenstates and eigenenergies.

A set of theoretical papers establishing the fundamentals of NHSE has triggered several experimental implementations, mostly in acoustics [30,31], mechanics [32,33], and electrical circuits [34–38]. Theoretical suggestions for NHSE systems in the field of photonics are based mostly on coupled ring resonators [39–41], exciton-polariton lattices [42–45], and photonic crystals [46–48]. According to our knowledge, experimental realizations of NHSE in photonics involve only discrete-time quantum walks in coupled optical fiber loops [49] and bulk optics [50], a synthetic frequency dimension in an optical ring resonator [51,52], and a single realization in a real space utilizing a chain of active ring resonators [53]. Therefore, the field still lacks a generic theoretical proposal of NHSE in real space that could be applied to a large range of platforms.

In this Letter, we present a generic implementation of nonreciprocity and NHSE, not related to fabricating microstructures or complicated lattices, and achievable in several platforms. The approach is based on coupling between spin and propagation direction by Rashba-Dresselhaus spin-orbit coupling (RDSOC) (existing for electrons [54,55], cold atoms [56], and photons [57]) and an in-plane effective magnetic field. By adding a spin-dependent lifetime [realized as well for electrons [58], cold atoms [59–61], and photons (see Supplemental Material [62] and also Ref. [63] therein)] we introduce non-Hermiticity into the system and obtain nonreciprocal

---

*Corresponding author: pavel.kokhanchik@uca.fr
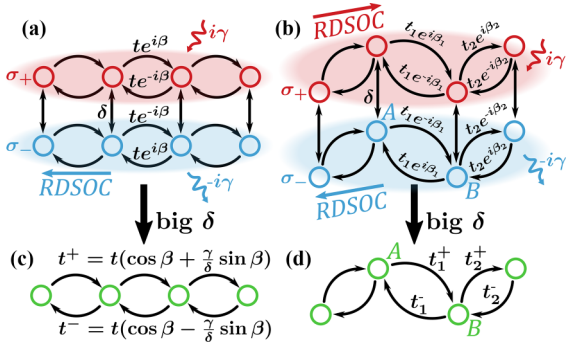
FIG. 1. (a), (b) Spinful monomer and SSH chains with RDSOC, (effective) in-plane magnetic field, and spin-dependent loss; (c) non-Hermitian HN and (d) SSH models.

FIG. 2. (a) Transition from Eq. (1) to Eq. (2) for a 40-site chain with an increase of δ displaying NHSE [blue (red) color shows the right (left) edge localization]; (b) normalized density of eigenstates for the lower band of (a) depending on the real part of the energy Re[E] and site number n; (c) BZ and GBZs of Eqs. (1) and (2); (d) PBC spectrum of Eq. (2), and OBC spectra of Eqs. (1) and (2). Parameters: $t = 1$, $\gamma = 1$, $\delta = 5$, $\beta = 0.2\pi$.

couplings. This allows us to model the HN and non-Hermitian SSH chains. Furthermore, with these ingredients, we obtain the NHSE without any lattice, in a single 1D trap. In a particular case of photonics, RDSOC, in-plane magnetic field, and spin-dependent lifetime are equivalent to optical activity [64], linear birefringence, and circular dichroism, respectively. The two first ingredients appear naturally in microcavities filled with liquid crystals (LCs) [57]. The circular dichroism can be produced by embedding a chiral optical absorber [65,66] or with spin-dependent gain [67]. We present realistic simulations showing NHSE using LC microcavity parameters. Finally, we show how the localization of skin modes can be controlled by an external voltage applied to LC microcavity, up to switching off the NHSE.

1D monomer chain. We start by considering the Hamiltonian of a spin-$\frac{1}{2}$ particle in a 1D monomer chain of coupled potential wells (sites), in the presence of RDSOC, in-plane (effective) magnetic field, and spin-dependent loss in the tight-binding approximation [Fig. 1(a)],

$$\hat{H}_1 = \sum_n \delta \hat{\sigma}_x a_n^\dagger a_n + i\gamma \hat{\sigma}_z a_n^\dagger a_n$$
$$+ t e^{i\beta \hat{\sigma}_z} a_{n+1}^\dagger a_n + t e^{-i\beta \hat{\sigma}_z} a_n^\dagger a_{n+1}, \quad (1)$$

with a_n ($a_n^\dagger$) the annihilation (creation) operator of a particle at lattice site n, $\hat{\sigma}_i$ the ith Pauli matrix, t the tunneling coefficient, and δ an in-plane magnetic field. The RDSOC can be represented as a constant gauge potential that enters the tunneling coefficient as a spin-dependent phase $\beta\hat{\sigma}_z$ (see details in Ref. [68]), the so-called Peierls phase [69]. The additional ingredient here is the on-site spin-dependent loss which was absent in our previous work [68] and which makes the Hamiltonian non-Hermitian. The average lifetime is not included in the Hamiltonian since it does not affect the physics related to the NHSE. The presence of the average lifetime will simply shift the whole spectrum in Fig. 2(d) in the region of the negative imaginary part Im[E] < 0, which is equivalent to a global decay of modes.

We first look at the limit of a large in-plane magnetic field: $|\delta| \gg |t|, |\gamma|$. The spin-subspace components of zero-order eigenstates are the ones of the $\hat{\sigma}_x$ matrix [the first term in Eq. (1)], while their perturbation is defined by the remaining terms. In this case the effective Hamiltonian (1) for

$|n\rangle \otimes |\sigma_x; -\rangle$ subspace reads

$$\hat{H}_1^{\text{eff}} = \hat{H}_{1,\text{on-site}}^{\text{eff}} + \hat{H}_{1,\text{NN}}^{\text{eff}} + \hat{H}_{1,\text{NNN}}^{\text{eff}}, \quad (2)$$

where

$$\hat{H}_{1,\text{NN}}^{\text{eff}} = \sum_n t^- a_n^\dagger a_{n+1} + t^+ a_{n+1}^\dagger a_n, \quad (3)$$

$$t^\pm = t\left(\cos\beta \pm \frac{\gamma}{\delta}\sin\beta\right). \quad (4)$$

$\hat{H}_{1,\text{on-site}}^{\text{eff}}$, $\hat{H}_{1,\text{NN}}^{\text{eff}}$, and $\hat{H}_{1,\text{NNN}}^{\text{eff}}$ stand for on-site, nearest-neighbor (NN), and next-nearest-neighbor (NNN) Hamiltonians, respectively (see exact formulas in the Supplemental Material [62]). As one can see from Eqs. (3) and (4), forward and backward tunneling coefficients $t^\pm$ differ by a factor $\frac{\gamma}{\delta}\sin\beta$. In this limit, the chain is equivalent to the nonreciprocal HN model up to the NNN tunnelings [Fig. 1(c)].

We next consider a 40-site chain. Figure 2(a) shows the real eigenenergies of the full Hamiltonian (1) versus δ. With increasing δ, a single band splits into two ($|n\rangle \otimes |\sigma_x; -\rangle$ and $|n\rangle \otimes |\sigma_x; +\rangle$ for big δ). Each of the two bands shows a strong localization of right eigenstates (from here on just eigenstates) on the edge of the chain (opposite edges for different bands). Figure 2(b) demonstrates for $\delta = 5$ the spatial distribution of modes of the lowest band, which confirms localization on the right edge. In a system where δ can be tuned experimentally, as in LC microcavities, NHSE can be turned on and off as shown by Fig. 2(a).

As discussed in the Introduction, the GBZ is a powerful tool to characterize the NHSE. In 1D Hermitian systems, the Brillouin zone (BZ) can be represented as the trigonometric circle $z = e^{ik}$, where k is a real wave number. In non-Hermitian systems, it is appropriate to consider an imaginary wave number characterizing exponentially localized

wave functions. This defines new eigenenergies where a portion of the imaginary part is transferred to the wave number, resulting in the GBZ represented by $z = re^{ik}$. If a part of the GBZ plotted on a complex z plane falls inside (outside) the BZ, corresponding eigenstates have $r < 1$ ($r > 1$) and would therefore experience the NHSE with localization on the right (left) side of a finite chain. The GBZs of the full Hamiltonian (1) and of the effective Hamiltonian (2) are shown in Fig. 2(c) by yellow and red lines, respectively. The GBZ of the full Hamiltonian (1) consists of two yellow solid lines corresponding to two bands localized on opposite edges. The GBZ of the reduced Hamiltonian (2) is in perfect agreement with the inner part of GBZ of full Hamiltonian (1), confirming their equivalence in this limit. In contrast to a pure HN model, red and yellow circles are not centered at $z = 0$ due to the presence of NNNs [Eq. (2) and Supplemental Material [62]].

The specificity of the non-Hermitian systems is that the spectra of infinite and finite systems differ profoundly. Indeed, the use of periodic boundary condition (PBC) requires considering only real wave numbers, and the imaginary part is carried by the complex eigenenergies. Figure 2(d) depicts the OBC spectra of Eq. (1) (yellow) and Eq. (2) (red) forming real-valued segments and the complex PBC spectrum of Eq. (2) (blue). One can see that the effective Hamiltonian (2) perfectly approximates the OBC spectrum of the lower-energy band of the full Hamiltonian (1). The complex PBC spectrum can be used to compute the non-Hermitian spectral winding number:

$$W_{E_b} := \frac{1}{2\pi} \oint_{BZ} \frac{d}{dz} \arg[H(z) - E_b] dz, \quad (5)$$

with $H(z)$ the PBC (Bloch) Hamiltonian, and $E_b \in \mathbb{C}$ a reference point. NHSE, therefore, occurs if the loop of the PBC spectrum encircles a nonzero area, which is clearly the case for the blue line in Fig. 2(d).

SSH chain. We continue by considering the SSH model—the celebrated model in topological physics first suggested to describe the dimer structure of a polyacetylene chain [21]. The chain contains two sublattices (A and B), and the Hamiltonian is written as [Fig. 1(b)]

$$\hat{H}_2 = \sum_n \delta \hat{\sigma}_x (a_{n,A}^\dagger a_{n,A} + a_{n,B}^\dagger a_{n,B})$$
$$+ i\gamma \hat{\sigma}_z (a_{n,A}^\dagger a_{n,A} + a_{n,B}^\dagger a_{n,B}) + (t_1 e^{i\beta_1 \hat{\sigma}_z} a_{n,B}^\dagger a_{n,A}$$
$$+ t_2 e^{-i\beta_2 \hat{\sigma}_z} a_{n,B}^\dagger a_{n+1,A} + \text{H.c.}), \quad (6)$$

where t_1 (t_2) is intracell (intercell) tunneling with a corresponding RDSOC phase β_1 (β_2), and all other parameters as in Eq. (1). By considering the $|\sigma_x; -\rangle$ subspace again, one can transform the Hamiltonian Eq. (6) to

$$\hat{H}_2^{\text{eff}} = \hat{H}_{2,\text{on-site}}^{\text{eff}} + \hat{H}_{2,\text{NN}}^{\text{eff}} + \hat{H}_{2,\text{NNN}}^{\text{eff}}, \quad (7)$$

$$\hat{H}_{2,\text{NN}}^{\text{eff}} = \sum_n t_1^+ a_{n,B}^\dagger a_{n,A} + t_1^- a_{n,A}^\dagger a_{n,B}$$
$$+ t_2^- a_{n,B}^\dagger a_{n+1,A} + t_2^+ a_{n+1,A}^\dagger a_{n,B}, \quad (8)$$

$$t_i^\pm = t_i \left(\cos \beta_i \pm \frac{\gamma}{\delta} \sin \beta_i \right). \quad (9)$$
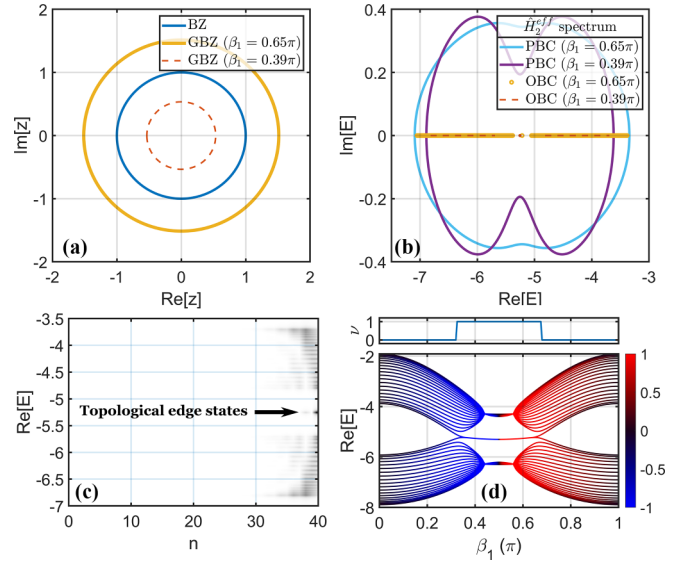
FIG. 3. (a) BZ and GBZs of Eq. (7) for two values of β_1; (b) PBC spectra of Eq. (7), and OBC spectra of Eq. (7) for two values of β_1, each showing two coinciding topological edge states; (c) normalized density of eigenstates of a 40-site chain depending on the real part of the energy Re[E] and site number n; (d) Eq. (7) real spectrum vs β_1 displaying NHSE [blue (red) color shows the right (left) edge localization] as well as a topological transition (bottom) confirmed by topological invariant ν (top). Parameters: $t_1 = 2$, $t_2 = 1$, $\gamma = 1$, $\delta = 5$, $\beta_2 = 0$.

Next, we investigate the case when $\beta_2 = 0$ for simplicity [Fig. 1(d)]. Consequently, the NNN term vanishes (see Supplemental Material [62]), and the chiral symmetry of the Hamiltonian (7) is restored. We stress that the NHSE is present for other values of β_2 as well. The Hamiltonian Eq. (7) then can be transformed into the conventional SSH Hamiltonian by a similarity transformation $\hat{H}_{\text{SSH}} = \hat{S} \hat{H}_2^{\text{eff}} \hat{S}^{-1}$ with $\hat{S} = \text{diag}\{1, rs, r, r^2 s, \dots, r^{N-1}, r^N s\}$, $r = \sqrt{t_1^- t_2^- / t_1^+ t_2^+}$, $s = \sqrt{t_1^+ / t_1^-}$, where $2N$ defines the number of lattice sites. The topology of the chain is then described by a Hermitian winding ν such that $\nu = 1$ for $|t_2^+ t_2^-| > |t_1^+ t_1^-|$, and $\nu = 0$ otherwise. The biorthogonal polarization invariant [18] shows the same transition for the initial non-Hermitian chain (7).

In Fig. 3(a) we show GBZs for two different values of β_1: $\beta_1 > \pi/2$ (yellow) and $\beta_1 < \pi/2$ (red). They indicate the NHSE effect with accumulation on different edges, which is also confirmed by Fig. 3(d), demonstrating a finite chain spectrum for different values of β_1 with a blue (red) color corresponding to the right (left) edge localization. The OBC spectra for the aforementioned values of β_1 are depicted in Fig. 3(b) (yellow and red lines) together with two PBC spectra (blue and purple lines). The individual dots between two bands of each OBC spectrum are the topological states. These topological states are localized at the edge of the chain (as the bulk states), but they are located inside the real gap of the OBC spectrum. They appear in Fig. 3(c), where we plot the normalized density of eigenstates versus the lattice site number. In the Hermitian limit ($\gamma \to 0$), the origin of the topological transition related to the formation of the edge states is the modulation of the tunneling amplitudes by the combination
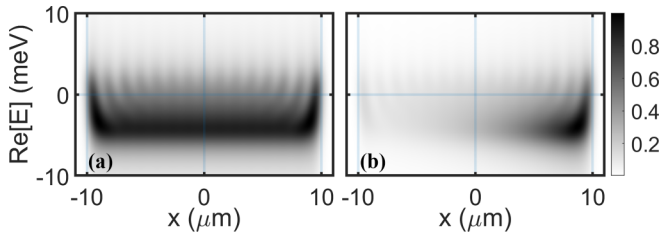
FIG. 4. Normalized eigenstate density for the lower-energy states of the potential well depending on the real part of the energy Re[E] and real-space coordinate x. Parameters: $d = 20$ µm, $U_0 = 10$ meV, $m = 1.6 \times 10^{-5} m_e$, m_e is the electron mass, $\alpha = 1$ meV µm, $\delta = 5$ meV, (a) $\gamma = 0$ meV and (b) $\gamma = 0.25$ meV.

of RDSOC β with the in-plane field δ, as described in our previous paper [68]. Here, this transition is modified by non-Hermiticity and described by the invariant ν plotted in the top panel of Fig. 3(d).

1D potential well. Finally, we show that the NHSE can be observed in a potential well, without the use of a lattice. To do so, we solve numerically the 1D spinor stationary Schrödinger equation with the Hamiltonian

$$\hat{H}_{\text{cont}}(x) = -\frac{\hbar^2}{2m}\frac{\partial^2}{\partial x^2}\hat{\sigma}_0 - 2i\alpha\frac{\partial}{\partial x}\hat{\sigma}_z$$
$$+ \delta\hat{\sigma}_x - i\gamma_0\hat{\sigma}_0 + i\gamma\hat{\sigma}_z + U(x)\hat{\sigma}_0, \quad (10)$$

with x the real-space coordinate, m the mass, γ_0 the common loss, γ the spin-dependent loss, and α the RDSOC magnitude. $U(x) = \{0,$ if $|x| < d; U_0$, otherwise$\}$ is the real-space potential with parameters $d = 20$ µm, $U_0 = 10$ meV. We plot the normalized eigenstate density for the Hermitian case $\gamma = 0$ meV in Fig. 4(a) and for the non-Hermitian case $\gamma = 0.25$ meV in Fig. 4(b). The parameters used correspond to realistic LC microcavities [57]. In particular, the broadening for every state is taken as $\gamma_0 = 2$ meV [70] in full width at half maximum which exceeds the quantization energy, so the individual lines are indistinguishable. Nevertheless, it does not prevent a clear observation of NHSE: One can see that the non-Hermiticity drives the density of all lowest eigenstates to the right edge of the well. A similar effect was suggested for cold atoms [71–73]. The inversion of either the RDSOC direction ($\alpha \to -\alpha$) or of the spin-dependent loss ($\gamma \to -\gamma$) changes the NHSE so that the eigenstates localize at another edge. This property provides the tunability of the effect. We provide additional analysis of the Hamiltonian (10) in the Supplemental Material [62] (see also Refs. [2,63,64,70,74,75] therein).

This effect can be explained again by considering one band $|\sigma_x; -\rangle$ in a limit of the large in-plane magnetic field δ. Then, the Hamiltonian (10) is rewritten as

$$\hat{H}_{\text{cont}}^{\text{eff}}(x) = E_0 + U(x) - \xi^2(\partial_x + \tau)^2, \quad (11)$$

with $E_0 = -\delta + \frac{\gamma^2}{2\delta} + (\frac{\alpha\gamma}{\xi\delta})^2$ constant energy shift, $\xi^2 = \frac{\hbar^2}{2m} - \frac{2\alpha^2}{\delta}$ kinetic energy scaling, and $\tau = \frac{\alpha\gamma}{\xi^2\delta}$ imaginary gauge

potential [76]. By considering the wave-function ansatz $\psi(x) = \varphi(x)e^{-\tau x}$, we arrive at a simple eigenvalue problem of a single spinless particle in a potential well with a wave function $\varphi(x)$:

$$\hat{H}_{\text{cont}}^{\text{eff}}(x)\varphi(x) = [E_0 + U(x) - \xi^2\partial_x^2]\varphi(x). \quad (12)$$

As one can see, τ^{-1} is a localization length of a wave function $\psi(x)$ and its finite value is a manifestation of NHSE. It is achieved only when α, γ, δ all have nonzero values, which confirms the necessity of each component in our model. The sign of τ is controlled by the combination of signs of α and γ.

As said above, one of the possible experimental realizations of this proposal is to use a photonic microcavity filled with LCs [57]. Here, the spin degree of freedom is represented by the photon polarization. The angle of the LC molecule director can be controlled via an external voltage. When the splitting between the modes of different linear polarization is big enough due to the rotation of LC molecules, two modes of opposite parity can come into resonance, giving rise to the RDSOC term in the Hamiltonian (10). A slight rotation of the LC director out of this resonance adds a splitting between these successive modes, entering the Hamiltonian as $\delta\hat{\sigma}_x$ (effective in-plane magnetic field). The presence of a chiral absorber or spin-dependent gain in a nonlinear system can create a polarization-dependent lifetime. The potential well can be created by structuring the mirror of the microcavity. This system possesses the continuous tunability of δ, as well as the possibility to switch α between zero and nonzero values. This allows one to tune the localization length τ^{-1} of NHSE or switch it on and off.

The realization of our proposal in the electronic systems is fully feasible as well. In the Supplemental Material [62] (see also Refs. [55,77–87] therein) we show that the Hamiltonian (10) can be achieved in a 1D nanowire composed of a ferromagnetic material and a semiconductor. In this case, a ferromagnet provides the necessary spin-dependent lifetime for electrons while a semiconductor offers the RDSOC and in-plane magnetic field. The calculation with experimental parameters shows the appearance of skin modes (see Supplemental Material [62]).

Conclusion. We propose a generic way to realize nonreciprocal tunnelings. It allows the implementation of models based on nonreciprocal couplings (HN model, non-Hermitian SSH, etc.). The method is based on combining RDSOC, (effective) in-plane magnetic field, and spin-dependent lifetime. Furthermore, we demonstrate that the NHSE can be observed even without a lattice. This proposal is feasible for different platforms in solid-state physics, cold atoms, or photonics. In particular, we simulate a realistic LC microcavity where NHSE can be tuned by voltage.

[1] E. J. Bergholtz, J. C. Budich, and F. K. Kunst, Exceptional topology of non-Hermitian systems, Rev. Mod. Phys. **93**, 015005 (2021).

[2] K. Kawabata, K. Shiozaki, M. Ueda, and M. Sato, Symmetry and Topology in Non-Hermitian Physics, Phys. Rev. X **9**, 041015 (2019).

[3] T. E. Lee, Anomalous Edge State in a Non-Hermitian Lattice, Phys. Rev. Lett. **116**, 133903 (2016).

[4] S. Yao and Z. Wang, Edge States and Topological Invariants of Non-Hermitian Systems, Phys. Rev. Lett. **121**, 086803 (2018).

[5] L. Feng, Y.-L. Xu, W. S. Fegadolli, M.-H. Lu, J. E. Oliveira, V. R. Almeida, Y.-F. Chen, and A. Scherer, Experimental demonstration of a unidirectional reflectionless parity-time metamaterial at optical frequencies, Nat. Mater. **12**, 108 (2013).

[6] J. Wiersig, Enhancing the Sensitivity of Frequency and Energy Splitting Detection by Using Exceptional Points: Application to Microcavity Sensors for Single-Particle Detection, Phys. Rev. Lett. **112**, 203901 (2014).

[7] J.-H. Park, A. Ndao, W. Cai, L. Hsu, A. Kodigala, T. Lepetit, Y.-H. Lo, and B. Kanté, Symmetry-breaking-induced plasmonic exceptional points and nanoscale sensing, Nat. Phys. **16**, 462 (2020).

[8] J. Wiersig, Response strengths of open systems at exceptional points, Phys. Rev. Res. **4**, 023121 (2022).

[9] B. Peng, Ş. K. Özdemir, M. Liertzer, W. Chen, J. Kramer, H. Yılmaz, J. Wiersig, S. Rotter, and L. Yang, Chiral modes and directional lasing at exceptional points, Proc. Natl. Acad. Sci. USA **113**, 6845 (2016).

[10] Y. Hatsugai, Chern number and edge states in the integer quantum Hall effect, Phys. Rev. Lett. **71**, 3697 (1993).

[11] M. Z. Hasan and C. L. Kane, Colloquium: Topological insulators, Rev. Mod. Phys. **82**, 3045 (2010).

[12] T. Ozawa, H. M. Price, A. Amo, N. Goldman, M. Hafezi, L. Lu, M. C. Rechtsman, D. Schuster, J. Simon, O. Zilberberg *et al.*, Topological photonics, Rev. Mod. Phys. **91**, 015006 (2019).

[13] D. Leykam, K. Y. Bliokh, C. Huang, Y. D. Chong, and F. Nori, Edge Modes, Degeneracies, and Topological Numbers in Non-Hermitian Systems, Phys. Rev. Lett. **118**, 040401 (2017).

[14] Y. Xiong, Why does bulk boundary correspondence fail in some non-Hermitian topological models, J. Phys. Commun. **2**, 035043 (2018).

[15] V. Martinez Alvarez, J. Barrios Vargas, M. Berdakin, and L. Foa Torres, Topological states of non-Hermitian systems, Eur. Phys. J.: Spec. Top. **227**, 1295 (2018).

[16] N. Hatano and D. R. Nelson, Localization Transitions in Non-Hermitian Quantum Mechanics, Phys. Rev. Lett. **77**, 570 (1996).

[17] S. Longhi, Nonadiabatic robust excitation transfer assisted by an imaginary gauge field, Phys. Rev. A **95**, 062122 (2017).

[18] F. K. Kunst, E. Edvardsson, J. C. Budich, and E. J. Bergholtz, Biorthogonal Bulk-Boundary Correspondence in Non-Hermitian Systems, Phys. Rev. Lett. **121**, 026808 (2018).

[19] S. Lieu, Topological phases in the non-Hermitian Su-Schrieffer-Heeger model, Phys. Rev. B **97**, 045106 (2018).

[20] C. Yin, H. Jiang, L. Li, R. Lü, and S. Chen, Geometrical meaning of winding number and its characterization of topological phases in one-dimensional chiral non-Hermitian systems, Phys. Rev. A **97**, 052115 (2018).

[21] W. P. Su, J. R. Schrieffer, and A. J. Heeger, Solitons in Polyacetylene, Phys. Rev. Lett. **42**, 1698 (1979).

[22] J. K. Asbóth, L. Oroszlány, and A. Pályi, A Short Course on Topological Insulators, *Lecture Notes in Physics*, Vol. 919 (Springer, Cham, 2016), p. 166.

[23] K. Yokomizo and S. Murakami, Non-Bloch Band Theory of Non-Hermitian Systems, Phys. Rev. Lett. **123**, 066404 (2019).

[24] E. Edvardsson, F. K. Kunst, and E. J. Bergholtz, Non-Hermitian extensions of higher-order topological phases and their biorthogonal bulk-boundary correspondence, Phys. Rev. B **99**, 081302(R) (2019).

[25] E. Edvardsson, F. K. Kunst, T. Yoshida, and E. J. Bergholtz, Phase transitions and generalized biorthogonal polarization in non-Hermitian systems, Phys. Rev. Res. **2**, 043046 (2020).

[26] Z. Gong, Y. Ashida, K. Kawabata, K. Takasan, S. Higashikawa, and M. Ueda, Topological Phases of Non-Hermitian Systems, Phys. Rev. X **8**, 031079 (2018).

[27] H. Shen, B. Zhen, and L. Fu, Topological Band Theory for Non-Hermitian Hamiltonians, Phys. Rev. Lett. **120**, 146402 (2018).

[28] F. Song, S. Yao, and Z. Wang, Non-Hermitian Topological Invariants in Real Space, Phys. Rev. Lett. **123**, 246801 (2019).

[29] K. Zhang, Z. Yang, and C. Fang, Correspondence between Winding Numbers and Skin Modes in Non-Hermitian Systems, Phys. Rev. Lett. **125**, 126402 (2020).

[30] X. Zhang, Y. Tian, J.-H. Jiang, M.-H. Lu, and Y.-F. Chen, Observation of higher-order non-Hermitian skin effect, Nat. Commun. **12**, 5377 (2021).

[31] L. Zhang, Y. Yang, Y. Ge, Y.-J. Guan, Q. Chen, Q. Yan, F. Chen, R. Xi, Y. Li, D. Jia *et al.*, Acoustic non-Hermitian skin effect from twisted winding topology, Nat. Commun. **12**, 6297 (2021).

[32] W. Wang, X. Wang, and G. Ma, Non-Hermitian morphing of topological modes, Nature (London) **608**, 50 (2022).

[33] A. Ghatak, M. Brandenbourger, J. Van Wezel, and C. Coulais, Observation of non-Hermitian topology and its bulk–edge correspondence in an active mechanical metamaterial, Proc. Natl. Acad. Sci. USA **117**, 29561 (2020).

[34] T. Helbig, T. Hofmann, S. Imhof, M. Abdelghany, T. Kiessling, L. Molenkamp, C. Lee, A. Szameit, M. Greiter, and R. Thomale, Generalized bulk–boundary correspondence in non-Hermitian topolectrical circuits, Nat. Phys. **16**, 747 (2020).

[35] T. Hofmann, T. Helbig, F. Schindler, N. Salgo, M. Brzezińska, M. Greiter, T. Kiessling, D. Wolf, A. Vollhardt, A. Kabaši *et al.*, Reciprocal skin effect and its realization in a topolectrical circuit, Phys. Rev. Res. **2**, 023265 (2020).

[36] S. Liu, R. Shao, S. Ma, L. Zhang, O. You, H. Wu, Y. J. Xiang, T. J. Cui, and S. Zhang, Non-Hermitian skin effect in a non-Hermitian electrical circuit, Research **2021**, 5608038 (2021).

[37] W. Zhang, F. Di, H. Yuan, H. Wang, X. Zheng, L. He, H. Sun, and X. Zhang, Observation of non-Hermitian many-body skin effects in Hilbert space, arXiv:2109.08334.

[38] D. Zou, T. Chen, W. He, J. Bao, C. H. Lee, H. Sun, and X. Zhang, Observation of hybrid higher-order skin-topological effect in non-Hermitian topolectrical circuits, Nat. Commun. **12**, 7201 (2021).

[39] S. Longhi, D. Gatti, and G. D. Valle, Robust light transport in non-Hermitian photonic lattices, Sci. Rep. **5**, 13376 (2015).

[40] X. Zhu, H. Wang, S. K. Gupta, H. Zhang, B. Xie, M. Lu, and Y. Chen, Photonic non-Hermitian skin effect and non-Bloch bulk-boundary correspondence, Phys. Rev. Res. **2**, 013280 (2020).

[41] Y. Song, W. Liu, L. Zheng, Y. Zhang, B. Wang, and P. Lu, Two-Dimensional Non-Hermitian Skin Effect in a Synthetic Photonic Lattice, Phys. Rev. Appl. **14**, 064076 (2020).

[42] S. Mandal, R. Banerjee, E. A. Ostrovskaya, and T. C. H. Liew, Nonreciprocal transport of exciton polaritons in a non-hermitian chain, Phys. Rev. Lett. **125**, 123902 (2020).

[43] H. Xu, K. Dini, X. Xu, R. Banerjee, S. Mandal, and T. C. H. Liew, Nonreciprocal exciton-polariton ring lattices, Phys. Rev. B **104**, 195301 (2021).

[44] S. Mandal, R. Banerjee, and T. C. Liew, From the topological spin-Hall effect to the non-Hermitian skin effect in an elliptical micropillar chain, ACS Photonics **9**, 527 (2022).

[45] X. Xu, R. Bao, and T. C. H. Liew, Non-Hermitian topological exciton-polariton corner modes, Phys. Rev. B **106**, L201302 (2022).

[46] J. Zhong, K. Wang, Y. Park, V. Asadchy, C. C. Wojcik, A. Dutt, and S. Fan, Nontrivial point-gap topology and non-Hermitian skin effect in photonic crystals, Phys. Rev. B **104**, 125416 (2021).

[47] K. Yokomizo, T. Yoda, and S. Murakami, Non-Hermitian waves in a continuous periodic model and application to photonic crystals, Phys. Rev. Res. **4**, 023089 (2022).

[48] Z. Fang, M. Hu, L. Zhou, and K. Ding, Geometry-dependent skin effects in reciprocal photonic crystals, Nanophotonics **11**, 3447 (2022).

[49] S. Weidemann, M. Kremer, T. Helbig, T. Hofmann, A. Stegmaier, M. Greiter, R. Thomale, and A. Szameit, Topological funneling of light, Science **368**, 311 (2020).

[50] L. Xiao, T. Deng, K. Wang, G. Zhu, Z. Wang, W. Yi, and P. Xue, Non-Hermitian bulk–boundary correspondence in quantum dynamics, Nat. Phys. **16**, 761 (2020).

[51] K. Wang, A. Dutt, K. Y. Yang, C. C. Wojcik, J. Vučković, and S. Fan, Generating arbitrary topological windings of a non-Hermitian band, Science **371**, 1240 (2021).

[52] K. Wang, A. Dutt, C. C. Wojcik, and S. Fan, Topological complex-energy braiding of non-Hermitian bands, Nature (London) **598**, 59 (2021).

[53] Y. G. Liu, Y. Wei, O. Hemmatyar, G. G. Pyrialakos, P. S. Jung, D. N. Christodoulides, and M. Khajavikhan, Complex skin modes in non-Hermitian coupled laser arrays, Light: Sci. Appl. **11**, 336 (2022).

[54] B. A. Bernevig, J. Orenstein, and S.-C. Zhang, Exact SU(2) Symmetry and Persistent Spin Helix in a Spin-Orbit Coupled System, Phys. Rev. Lett. **97**, 236601 (2006).

[55] J. D. Koralek, C. P. Weber, J. Orenstein, B. A. Bernevig, S.-C. Zhang, S. Mack, and D. Awschalom, Emergence of the persistent spin helix in semiconductor quantum wells, Nature (London) **458**, 610 (2009).

[56] Y.-J. Lin, K. Jiménez-García, and I. B. Spielman, Spin–orbit-coupled Bose–Einstein condensates, Nature (London) **471**, 83 (2011).

[57] K. Rechcińska, M. Król, R. Mazur, P. Morawiak, R. Mirek, K. Łempicka, W. Bardyszewski, M. Matuszewski, P. Kula, W. Piecek et al., Engineering spin-orbit synthetic Hamiltonians in liquid-crystal optical cavities, Science **366**, 727 (2019).

[58] M. Weinelt, A. Schmidt, M. Pickel, and M. Donath, Spin-polarized image-potential-state electrons as ultrafast magnetic sensors in front of ferromagnetic surfaces, Prog. Surf. Sci. **82**, 388 (2007).

[59] S. Tojo, T. Hayashi, T. Tanabe, T. Hirano, Y. Kawaguchi, H. Saito, and M. Ueda, Spin-dependent inelastic collisions in spin-2 Bose-Einstein condensates, Phys. Rev. A **80**, 042704 (2009).

[60] Z. Ren, D. Liu, E. Zhao, C. He, K. K. Pak, J. Li, and G.-B. Jo, Chiral control of quantum states in non-Hermitian spin–orbit-coupled fermions, Nat. Phys. **18**, 385 (2022).

[61] J. Qin, L. Zhou, and G. Dong, Imaginary spin-orbital coupling in parity-time symmetric systems with momentum-dependent gain and loss, New J. Phys. **24**, 063025 (2022).

[62] See Supplemental Material at http://link.aps.org/supplemental/10.1103/PhysRevB.108.L041403 for whole formulas of effective Hamiltonians (2) and (7), details about circular dichroism in the GaAs microcavity, symmetries of the Hamiltonian (10), discussion of the effect of Zeeman splitting and linear polarization lifetime imbalance, as well as a possible realization of the NHSE in the electronic system.

[63] A. Gianfrate, O. Bleu, L. Dominici, V. Ardizzone, M. De Giorgi, D. Ballarini, G. Lerario, K. West, L. Pfeiffer, D. Solnyshkov, D. Sanvitto, and G. Malpuech, Measurement of the quantum geometric tensor and of the anomalous Hall drift, Nature (London) **578**, 381 (2020).

[64] J. Ren, Q. Liao, F. Li, Y. Li, O. Bleu, G. Malpuech, J. Yao, H. Fu, and D. Solnyshkov, Nontrivial band geometry in an optically active system, Nat. Commun. **12**, 689 (2021).

[65] S. Y. Han, R. K. Mow, A. K. Bartholomew, F. Ng, M. L. Steigerwald, X. Roy, C. Nuckolls, and R. A. Wiscons, Broadband chiral absorbance of visible light, J. Am. Chem. Soc. **144**, 5263 (2022).

[66] G. Long, R. Sabatini, M. I. Saidaminov, G. Lakhwani, A. Rasmita, X. Liu, E. H. Sargent, and W. Gao, Chiral-perovskite optoelectronics, Nat. Rev. Mater. **5**, 423 (2020).

[67] N. Carlon Zambon, P. St-Jean, M. Milićević, A. Lemaître, A. Harouri, L. Le Gratiet, O. Bleu, D. Solnyshkov, G. Malpuech, I. Sagnes et al., Optically controlling the emission chirality of microlasers, Nat. Photonics **13**, 283 (2019).

[68] P. Kokhanchik, D. Solnyshkov, T. Stöferle, B. Piętka, J. Szczytko, and G. Malpuech, Modulated Rashba-Dresselhaus Spin-Orbit Coupling for Topology Control and Analog Simulations, Phys. Rev. Lett. **129**, 246801 (2022).

[69] R. Peierls, Zur theorie des diamagnetismus von leitungselektronen, Z. Phys. **80**, 763 (1933).

[70] M. Król, I. Septembre, P. Oliwa, M. Kędziora, K. Łempicka-Mirek, M. Muszyński, R. Mazur, P. Morawiak, W. Piecek, P. Kula et al., Annihilation of exceptional points from different dirac valleys in a 2D photonic system, Nat. Commun. **13**, 5340 (2022).

[71] S. Guo, C. Dong, F. Zhang, J. Hu, and Z. Yang, Theoretical prediction of a non-Hermitian skin effect in ultracold-atom systems, Phys. Rev. A **106**, L061302 (2022).

[72] L. Zhou, H. Li, W. Yi, and X. Cui, Engineering non-Hermitian skin effect with band topology in ultracold gases, Commun. Phys. **5**, 252 (2022).

[73] H. Li, X. Cui, and W. Yi, Non-Hermitian skin effect in a spin-orbit-coupled Bose-Einstein condensate, JUSTC **52**, 2 (2022).

[74] A. V. Nalitov, D. D. Solnyshkov, and G. Malpuech, Polariton ℤ Topological Insulator, Phys. Rev. Lett. **114**, 116401 (2015).

[75] L. Polimeno, G. Lerario, M. De Giorgi, L. De Marco, L. Dominici, F. Todisco, A. Coriolano, V. Ardizzone, M. Pugliese, C. T. Prontera et al., Tuning of the berry curvature in 2D perovskite polaritons, Nat. Nanotechnol. **16**, 1349 (2021).

[76] S. Longhi, Non-Hermitian skin effect beyond the tight-binding models, Phys. Rev. B **104**, 125109 (2021).

[77] S. Vaitiekėnas, Y. Liu, P. Krogstrup, and C. Marcus, Zero-bias peaks at zero magnetic field in ferromagnetic hybrid nanowires, Nat. Phys. **17**, 43 (2021).

[78] Y. Liu, S. Vaitiekenas, S. Martí-Sánchez, C. Koch, S. Hart, Z. Cui, T. Kanne, S. A. Khan, R. Tanta, S. Upadhyay *et al.*, Semiconductor–ferromagnetic insulator–superconductor nanowires: Stray field and exchange field, Nano Lett. **20**, 456 (2020).

[79] J. Cayao, Exceptional degeneracies in non-Hermitian Rashba semiconductors, J. Phys.: Condens. Matter **35**, 254002 (2023).

[80] S. Giglberger, L. E. Golub, V. V. Bel'kov, S. N. Danilov, D. Schuh, C. Gerl, F. Rohlfing, J. Stahl, W. Wegscheider, D. Weiss, W. Prettl, and S. D. Ganichev, Rashba and Dresselhaus spin splittings in semiconductor quantum wells measured by spin photocurrents, Phys. Rev. B **75**, 035327 (2007).

[81] F. Passek, M. Donath, K. Ertl, and V. Dose, Longer Living Majority than Minority Image State at Fe(110), Phys. Rev. Lett. **75**, 2746 (1995).

[82] M. Aeschlimann, M. Bauer, S. Pawlik, W. Weber, R. Burgermeister, D. Oberli, and H. C. Siegmann, Ultrafast Spin-Dependent Electron Dynamics in fcc Co, Phys. Rev. Lett. **79**, 5158 (1997).

[83] M. Donath, C. Math, M. Pickel, A. Schmidt, and M. Weinelt, Realization of a spin-polarized two-dimensional electron gas via image-potential-induced surface states, Surf. Sci. **601**, 5701 (2007).

[84] I. Mihai Miron, G. Gaudin, S. Auffret, B. Rodmacq, A. Schuhl, S. Pizzini, J. Vogel, and P. Gambardella, Current-driven spin torque induced by the Rashba effect in a ferromagnetic metal layer, Nat. Mater. **9**, 230 (2010).

[85] X. Wang and A. Manchon, Diffusive Spin Dynamics in Ferromagnetic Thin Films with a Rashba Interaction, Phys. Rev. Lett. **108**, 117201 (2012).

[86] D. Pesin and A. H. MacDonald, Quantum kinetic theory of current-induced torques in Rashba ferromagnets, Phys. Rev. B **86**, 014416 (2012).

[87] H. Yang, G. Chen, A. A. Cotta, A. T. N'Diaye, S. A. Nikolaev, E. A. Soares, W. A. Macedo, K. Liu, A. K. Schmid, A. Fert *et al.*, Significant Dzyaloshinskii–Moriya interaction at graphene–ferromagnet interfaces due to the Rashba effect, Nat. Mater. **17**, 605 (2018).